Iranian Polymer Journal (2022) 31:869–882
https://doi.org/10.1007/s13726-022-01045-9

ORIGINAL RESEARCH

Non-isothermal crystallization kinetics of poly(phthalazinone ether sulfone)/MC nylon 6 in-situ composites

Huimei Yao[1] · Wei Li[1] · Zhen Zeng[1] · Tao Wang[1] · Jingrui Zhu[1] · Zhiyong Lin[2]

Received: 25 September 2021 / Accepted: 15 January 2022 / Published online: 15 March 2022

Abstract

Non-isothermal crystallization behaviors and non-isothermal crystallization kinetics of poly(phthalazinone ether sulfone) (PPES)/MC nylon 6 in-situ composites prepared by anionic ring-opening polymerization were explored by differential scanning calorimetry (DSC) at various cooling rates. The Fourier transform infrared spectroscopy (FTIR) results confirmed that PPES/MC nylon 6 in-situ composites were successfully synthesized. The scanning electron microscopy (SEM) results demonstrated that PPES particles were well dispersed, at micron levels, in the MC nylon 6 matrix. The DSC results showed that inclusion of PPES to MC nylon 6 increased the crystallinity, while the crystallization rate was reduced. Crystallization kinetic analysis by Jeziorny model exhibited two levels of primary and secondary crystallization mechanisms for all samples, and the lower values of Z_c for the in-situ composites as compared to those of MC nylon 6 indicated that MC nylon 6 crystallization process becomes slower in the presence of PPES. The $F(T)$ values of the composites were generally higher as compared to those of pure MC nylon 6, indicating that the interaction between PPES and MC nylon 6 matrix was stronger and the movement of the polymer molecular chain was difficult. Moreover, activation energies of crystallization of the in-situ composites were lower than that of MC nylon 6. Analysis of data founded on theoretical models revealed that PPES acts as a nucleating agent in the nucleation stage and restricts the movement of chain segments for MC nylon 6 during crystal growth.

Graphical abstract

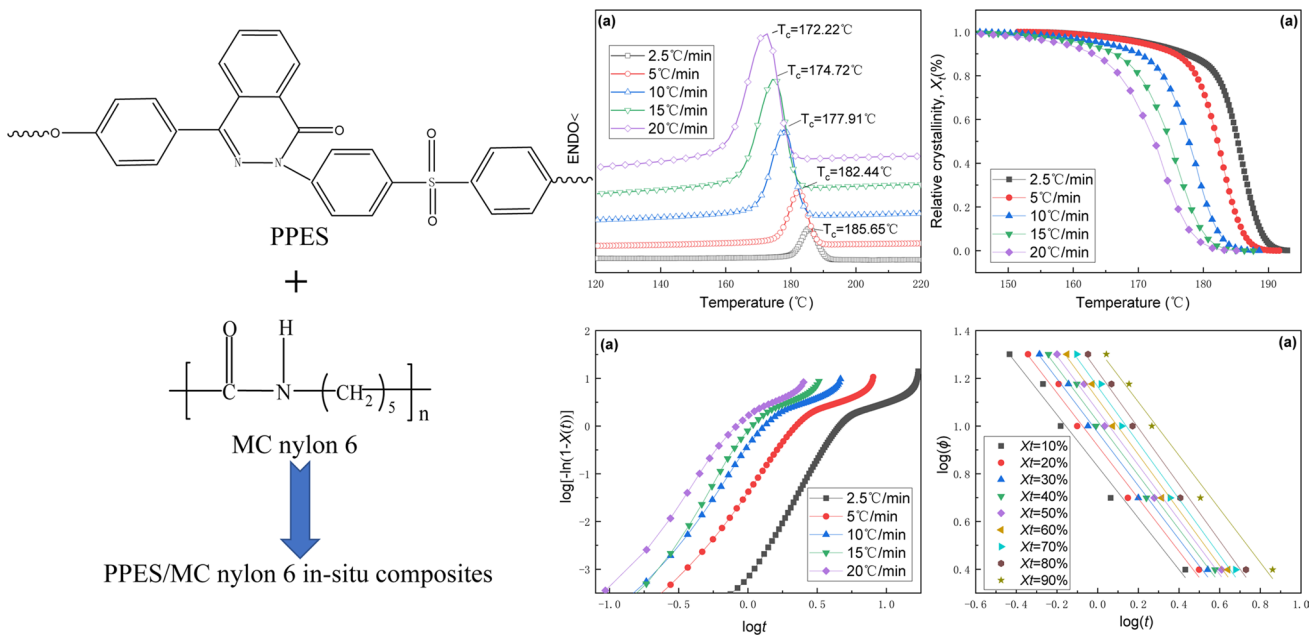

Extended author information available on the last page of the article

Keywords Poly(phthalazinone ether sulfone) (PPES) · MC nylon 6 · In-situ composites · Non-isothermal crystallization kinetics · Crystallization activation energy

Introduction

MC nylon 6 is a widely used semi-crystalline engineering plastic for many industrial applications due to its low polymerization temperature, simple preparation process, high molecular weight, high mechanical strength, and excellent self-lubrication performance. However, it suffers from inferior properties, such as high water absorption due to strong polarity, poor toughness at low temperature, poor dimensional stability, and inferior heat resistance, when used as a high-temperature engineering plastic [1]. The main approaches to overcome these problems are to modify MC nylon 6by filling, reinforcing, copolymerization, blending, compounding, and other methods [2, 3]. In this context, some studies have been done on exploring the properties of blends comprising MC nylon 6 prepared through in-situ dispersion polymerization. Zhang et al. performed a comprehensive study on the influence of different pretreatment methods and the addition amount of cellulose nanocrystalline (CNC) on the properties of MC nylon 6 in-situ composites. They concluded that with the increase of the amount of CNC, the crystallinity showed an upward trend, with higher crystallization temperature and narrower half peak width. The tensile strength, flexural strength and flexural elastic modulus of MCPA6/CNC in-situ composite were higher than those of pure MCPA6, respectively [1]. Yang et al. studied the structure, thermal properties, mechanical properties and morphologies of the composites, and they concluded that the thermal properties of MC nylon 6 components in the composites were similar to those of commercial nylon 6, and the CF was uniformly distributed in the matrix and fully impregnated by MC nylon 6 [4]. Taki and coworkers investigated the effect of thermal annealing on the crystallinity and mechanical properties of PA6, textile glass fiber-reinforced PA6 (GF-PA6), and carbon fiber-reinforced PA6 (CF-PA6) (40% by vol). They showed that the crystallinity, tensile modulus, and strength of PA6 were improved by thermal annealing. The crystallinity of GF-PA6 was not improved, but the tensile modulus and strength were slightly improved. The crystallinity of CF-PA6 decreased, but the tensile modulus and strength improved [5].

Poly(phthalazinone ether sulfone) (PPES) containing phthalazinone structure as a variety of engineering thermoplastic polymers has been extensively applied in electronics, biomedical and automotive fields due to its excellent heat resistance (its glass transition temperature is up to 305℃), chemical corrosion resistance, dielectric properties, and mechanical properties [6]. Therefore, it has a broad prospect in the application of high-performance resin matrix composites. Liu et al. prepared carbon fiber-reinforced poly(CF/PPEK) and carbon fiber-reinforced poly(CF/PPES) unidirectional composites using the pre-impregnated hot compression molding process. They studied the properties and changing law of the holding ratio of the strength and modulus of the high-performance thermoplastic composites under high temperature. They found that the retention of extension strength and bending strength and their modulus were above 60% below 250 °C, which had a super high loading capacity [7]. Zhang [8] studied the high and low temperature mechanics performance and interface of high-performance thermoplastic resin–PPEK, PPES and their composites. He showed that PPEK, PPES and their composites also had good bend performance under high and low temperatures, and the discrimination between them was minor. Zhang prepared PPES-*b*-MCPA6 block copolymer and used it as a compatibilizer for PPES/PA6 systems. He founded that in PPES/PA6 systems, when they joined the block copolymer, the dispersion of PPES phase in the matrix PA6 increased, and at the same time the cohesive force between the PPES and PA6 interface increased, as well as the mechanical properties could increase 18–22%. The thermal decomposition temperature was improved by addition of copolymerization [9].

In this context, several efforts will be made to improve the comprehensive performance of MC nylon 6 by inclusion of PPES, especially the inferior heat resistance of MC nylon 6. Therefore, a series of PPES/MC nylon 6 in-situ composites with different contents were first prepared by anionic in-situ polymerization.

A review of the literature shows that there are no reports on the crystallization behavior of PPES/MC nylon 6 in-situ composites. On the other hand, MC nylon 6 as a semi-crystalline polymer exhibits highly sensitive crystallization kinetic toward inclusion of additives. PPES may change the degree of crystallinity of MC nylon 6 as well, which may in turn affect its properties. Considering that non-isothermal crystallization is consistent with practical industrial processing techniques, such as extrusion and injection molding, the corresponding research has more practical significance than isothermal crystallization studies. The main purpose of this work is to evaluate the influence of PPES inclusion on the crystallization kinetic of MC nylon 6. Using Jeziorny and Mo models, the non-isothermal crystallization kinetics of the developed in-situ composite systems were explored. The crystallization activation energies were also calculated. It is suggested that the results can provide a theoretical foundation to direct the molding process and regulate the performance of PPES/MC nylon 6 in-situ composites.

Experimental

Materials

Industrial grade poly(phthalazinone ether sulfone) (PPES) was prepared from Jida High-tech Materials Co., Ltd. (China) and dried in a vacuum drying oven at 100 °C for 24 h before use. Polymerization grade caprolactam and sodium hydroxide (AR) were obtained from Yueyang Petrochemical Plant (China) and Shanghai No.3 Chemical Reagent Factory (China), respectively. 2,4-Toluene diisocyanate (2,4-TDI) (CP), reserved by vacuum distillation, was acquired from Shanghai No.3 Chemical Reagent Factory (China).

Sample preparation

Caprolactam monomer (250 g) was added into a glass test tube and heated up to 150℃ in an oil bath. After melting, sodium hydroxide was added as a catalyst and vacuumed under reduced pressure for 30 min to ensure as much water removal as possible. After stopping the vacuum pump, PPES particles were dispersed evenly in molten caprolactam by magnetic stirring after drying in vacuum, and then pumped into the vacuum so that the system would not bubble. The magnetic stirring was then stopped and the 2,4-toluene diisocyanate cocatalyst was added and stirred rapidly and uniformly. The temperature was kept constant at 150 °C for 60 min, and by removing the system it was cooled naturally to room temperature. Finally, PPES/MC nylon 6 in-situ composites were prepared by anion ring-opening polymerization. The samples of pure MC nylon 6 (S0) and PPES with the mass percentage of 2.0% (S1), 4.0% (S2), 6.0% (S3), and 8.0% (S4) were selected for the study. The schematic diagram of molecular structure and reaction process is shown in Fig. 1.

Testing and characterization

The non-isothermal crystallization behavior and crystallization kinetics were studied with the assistance of a differential scanning calorimeter (TA-2910, USA). The samples with a mass of 3–4 mg were rapidly heated from the ambient temperature to 250 °C, and maintained at 250 °C for 5 min to remove the previous thermal history, under nitrogen atmosphere. Subsequently, all the samples were cooled down from the melting temperature to the ambient temperature at varying cooling rates (2.5, 5, 10, 15 and 20 °C/min), and the changes in enthalpy value of the samples with temperature during crystallization were measured. The DSC instrument was calibrated with indium at each cooling rate used herein.

The FTIR spectra were obtained using a Nicolet Company $Nexus_{TM}$ IR spectrophotometer with KBr pellets with 32 scans.

The phase morphology of MC nylon 6 and PPES/MC nylon 6 in-situ composites was analyzed by a Hitachi S-3500N scanning electron microscope (SEM). For this purpose, the samples were fractured in liquid nitrogen, and the fractured sections were etched with chloroform, followed by a gold sputtering process.

Results and discussion

Fourier transform infrared spectroscopy (FTIR)

FTIR experiments were performed to detect the chemical structure of the PPES, MC nylon 6 and PPES/MC nylon 6 in-situ composites. As shown in Fig. 2a, the absorption at 3068.25 cm^{-1} in the PPES FTIR spectrum is due to the C–H stretching vibration of the benzene ring, the two distinctive absorption peaks at 1327.97 and 1310.47 cm^{-1} are related to the O=S=O asymmetric stretching vibration absorption (usually split into two peaks), the peak at 1151.53 cm^{-1} belongs to the symmetric stretching vibration of O=S=O,

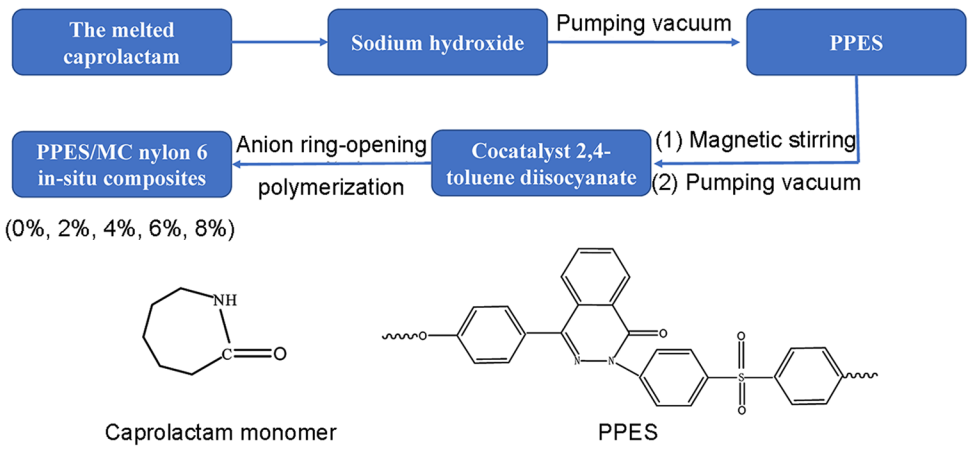

Fig. 1 Schematic diagram of the molecular structure and reaction process

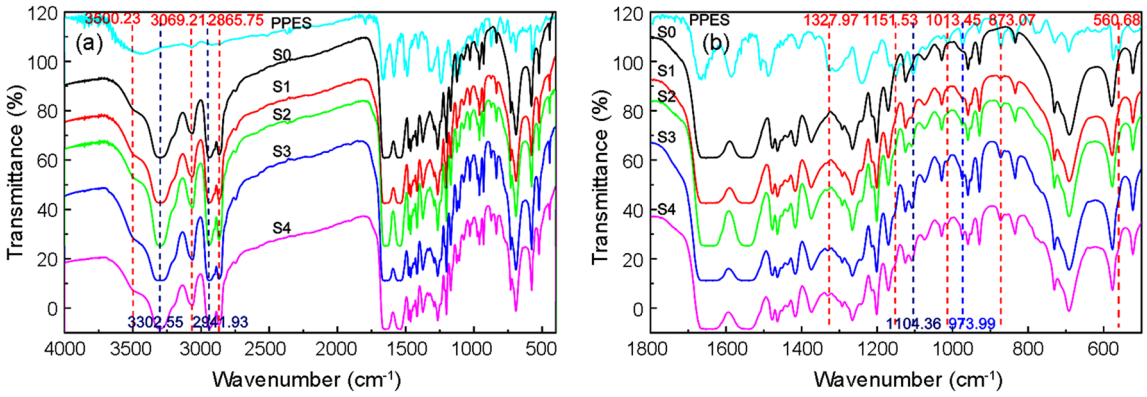

Fig. 2 FTIR spectra of PPES, MC nylon 6 and PPES/MC nylon 6 in-situ composites: **a** overall view; and **b** partial enlarged figure

the peaks at 1240.28 and 1166.37 cm^{-1} are ascribed to the asymmetric and symmetric stretching vibrations of aryl ether, respectively, the peak at 1585.95 cm^{-1} is due to the C=C double bond stretching vibration of the benzene ring, and the peaks at 1201.90, 1086.93 and 1013.66 $cm^{-1}$are attributed to the in-plane bending vibration of the benzene ring. The characteristic peaks in the PPES infrared spectrum show that they are consistent with the PPES molecular structure. As can be seen from Fig. 2b, compared with the infrared spectrum of MC nylon 6 (S0), there are characteristic peaks representing PPES molecular structure in PPES/MC nylon 6 in-situ composites, which are located at 1327.97, 1151.53, 1104.36, 1013.45, 973.99, 873.07 and 560.68 cm^{-1}, respectively. With the increase of PPES content, the peak strength gradually increases. From the results of FTIR it indicates that PPES/MC nylon 6 in-situ composites have been successfully synthesized.

Morphology of the PEES/MC nylon 6 composites

SEM analysis was used to investigate the phase morphology of PPES/MC nylon 6 in-situ composites. The effect of blending ratio on the blend morphology can be inferred from the comparison of Fig. 3, which reveals the blend morphology of PPES/MC nylon 6 in-situ composites. All samples exhibit refined and uniform biphasic morphology in which PPES particles are well dispersed, at micron levels, in the MC nylon 6 matrix. The good compatibility of these two polymers is due to the presence of a certain hydrogen bond interaction between PPES and molten caprolactam, which was analyzed in our previous study [10]. As expected, an increase in PPES content of the composite from 2 to 8% (by weight) increases the size of PPES particles due to coalescence phenomenon.

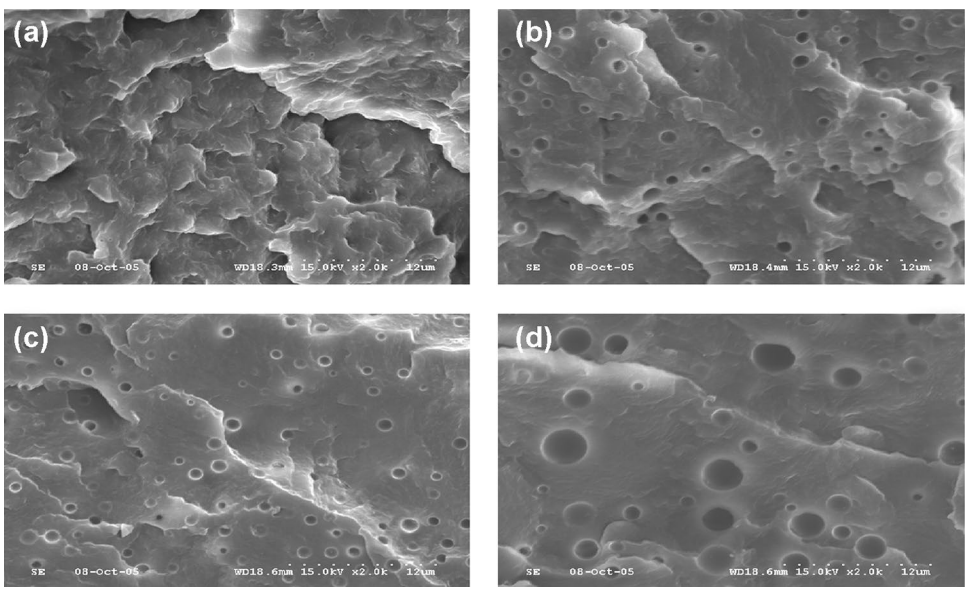

Fig. 3 SEM photographs of PPES/MC nylon 6 in-situ composites etched by chloroform: **a** S1×2000; **b** S2×2000; **c** S3×2000; and **d** S4×2000

Non-isothermal crystallization behavior

The DSC exotherms of MC nylon 6 and its in-situ composites obtained at different cooling rates are presented in Fig. 4, whereas the DSC data for all the studied samples are tabulated in Table 1. From the figure, generally it is seen that with increasing the cooling rate, the crystallization peaks shift toward lower temperatures and the peak shapes become wider due to the increased test speed, showing that when the cooling rate becomes slower, the molecular chains have enough time to arrange regularly and form more perfect and uniform crystals [11–13]. The in-situ blending of PEES with MC nylon6 and increasing the PPES content of the composites result in an increase of the T_{ini} (initial crystallization temperature) and a small reduction of the T_c (crystallization peak temperature) of the MC nylon 6. This is mainly due to the fact that the presence of PPES particles being at solid state at the crystallization temperature of MC nylon 6, can act as a nucleating agent at the beginning of crystallization of MC nylon 6. In addition, there are present a certain hydrogen bond interaction between PPES and molten MC nylon 6, analyzed in our previous study [10], which can hamper the mobility of the MC nylon 6 chains. With increasing PPES content, large numbers, small size imperfect crystals were formed. This finding is consistent with that of Alvaredo et al., who characterized the effect of graphene nanosheets content on the melt crystallization of PEEK composites using differential scanning calorimetry. The DSC data revealed a dual action of graphene: one was that the nucleation effect caused crystallization to start at a higher temperature; the other was that the reduction of the mobility of the polymer segments made the overall crystallization time longer [14].

The degree of crystallinity (X_c) of the composites can be obtained from Eq. 1:

$$X_c = \left\{\Delta H_c / \left[(1-\varphi)\Delta H_m^0\right]\right\} \times 100\%, \quad (1)$$

where ΔH_c is the crystallization heat of the sample, ΔH_m^0 is the melting enthalpy of complete crystallization of MC nylon 6 (230 J/g [15]) and φ is the mass percentage of PPES.

From Table 1, it is also seen that the X_c values for most of the studied samples decrease slightly with an increase in the cooling rate. While the increases in the PPES content increase the X_c value of MC nylon 6 slightly. ΔW values (half height–weight of crystallization peak) increase with an increase in the cooling rate, while they first decrease and then increase with the increase in PPES content.

Several important parameters can be extracted from the DSC thermograms to further shed light on the crystallization kinetics of the developed systems. One of these parameters is the relative degree of crystallinity at a certain temperature denoted as $X(T)$. This parameter is obtained based on the following equation:

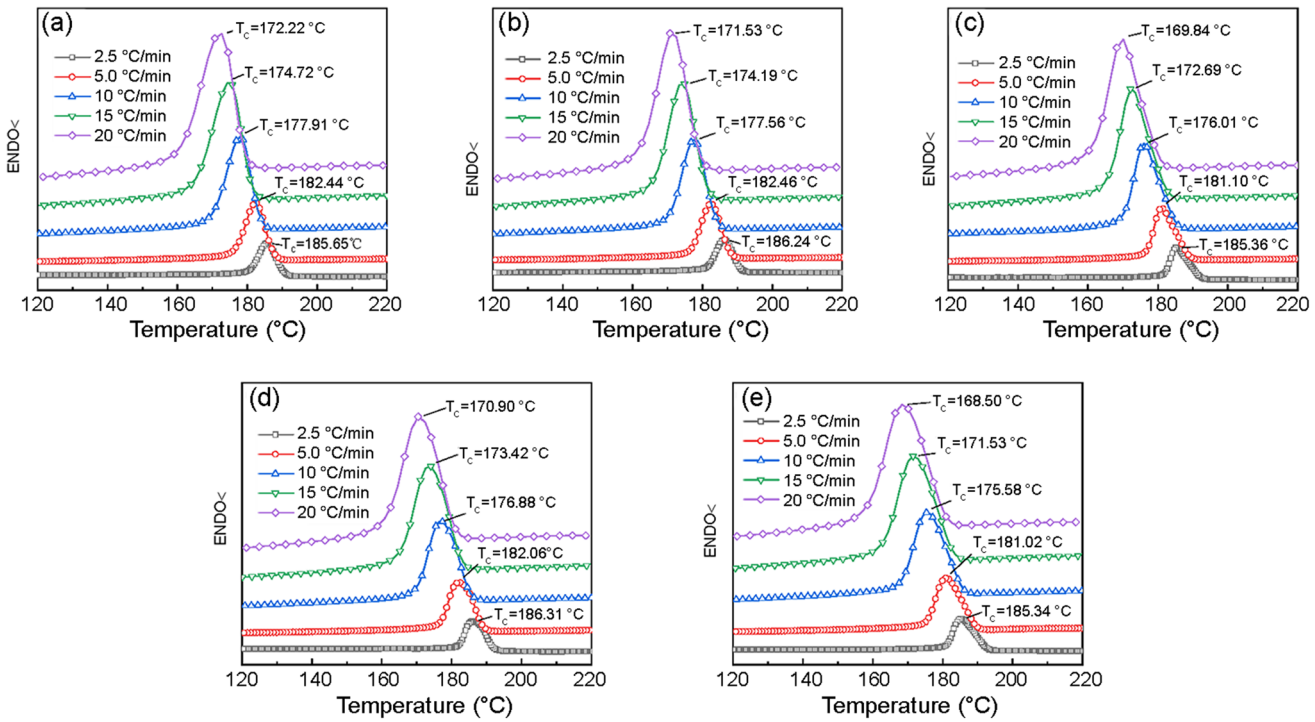

Fig. 4 DSC cooling curves at different cooling rates: **a** S0; **b** S1; **c** S2; **d** S3; and **e** S4

Table 1 Non-isothermal crystallization parameters of MC nylon 6 and PPES/MC nylon 6 in-situ composites at different cooling rates

Samples	ϕ (℃/min)	T_{ini} (℃)	T_c (℃)	ΔW (℃)	ΔH_c (J/g)	X_c (%)
S0	2.5	190.40	185.65	5.55	51.91	22.57
	5	187.46	182.44	6.39	55.25	24.02
	10	183.50	177.91	7.84	51.46	22.37
	15	180.98	174.72	9.28	51.12	22.23
	20	179.05	172.22	10.64	49.05	21.33
S1	2.5	190.71	186.24	5.40	64.72	28.71
	5	187.71	182.46	6.43	58.92	26.14
	10	183.71	177.56	7.69	53.21	23.61
	15	180.92	174.19	8.61	52.30	23.20
	20	178.81	171.53	9.56	51.39	22.80
S2	2.5	192.11	185.36	5.65	51.81	23.46
	5	188.61	181.10	6.74	54.76	24.80
	10	184.34	176.01	7.96	51.58	23.36
	15	181.69	172.69	9.11	49.98	22.64
	20	179.75	169.84	10.17	49.31	22.33
S3	2.5	191.81	186.31	6.44	50.48	23.35
	5	188.85	182.06	7.83	56.51	26.14
	10	185.17	176.88	9.45	50.99	23.58
	15	182.70	173.42	10.62	50.45	23.33
	20	180.76	170.90	11.76	49.38	22.84
S4	2.5	192.55	185.34	6.71	50.07	23.66
	5	189.59	181.02	8.29	50.92	24.06
	10	185.73	175.58	10.27	47.72	22.55
	15	183.06	171.53	11.84	49.59	23.44
	20	180.89	168.50	13.22	49.37	23.33

ϕ cooling rate, T_{ini} the temperature at the onset of crystallization, T_c peak temperature of crystallization, ΔW half height–weight of crystallization peak, ΔH_c the heat of crystallization, X_c degree of crystallinity

$$X(T) = \frac{\int_{T_0}^{T} \frac{dH_c(T)}{dT} dt}{\int_{T_0}^{T_f} \frac{dH_c(T)}{dT} dT} = \frac{A_T}{A_{total}}, \quad (2)$$

where T_0 and T_f are the initial and final temperatures of the crystallization process, respectively, obtained from the DSC crystallization peaks. Based on Eq. 2 and using experimental data, the variations of the relative crystallinity ($X(T)$) against temperature for the neat MC nylon 6 and PPES/MC nylon6 in-situ composites at different cooling rates were calculated, and the results are depicted in Fig. 5, respectively:

$$t = (T_0 - T)/\phi. \quad (3)$$

Based on Eq. 3, the crystallization temperature can switch to the crystallization time [16]. Where ϕ and T_0 are the cooling rate and the initial temperature of the crystallization process, respectively. T is the instant temperature at time t within the crystallization zone.

By combining Eqs. 2 and 3, one can calculate the relative degree of crystallinity at any given time, that is, $X(t)$ can be obtained from Eq. 4 [17]. Accordingly, the variations of $X(t)$ against time for a neat MC nylon 6 and PPES/MC nylon 6 in-situ composites at different cooling rates were calculated and the results are depicted in Fig. 6. Based on the results presented in Figs. 5 and 6, using different existing models, detailed crystallization kinetic analyses were performed, and the results are presented in the subsequent sections:

$$X(t) = \frac{X_c(t)}{X_c(t=\infty)} = \frac{\int_0^t \frac{dH_c(t)}{d(t)} dt}{\int_0^{t=\infty} \frac{dH_c(t)}{dt} dt} = 1 - \exp(-Zt^n). \quad (4)$$

Non-isothermal crystallization kinetics

Many works have reported on the study of non-isothermal crystallization kinetics of polymer systems by DSC method [18–33]. Starting from the Avrami equation for treating isothermal crystallization and considering the characteristics of non-isothermal crystallization, some methods for treating non-isothermal crystallization kinetics have been obtained

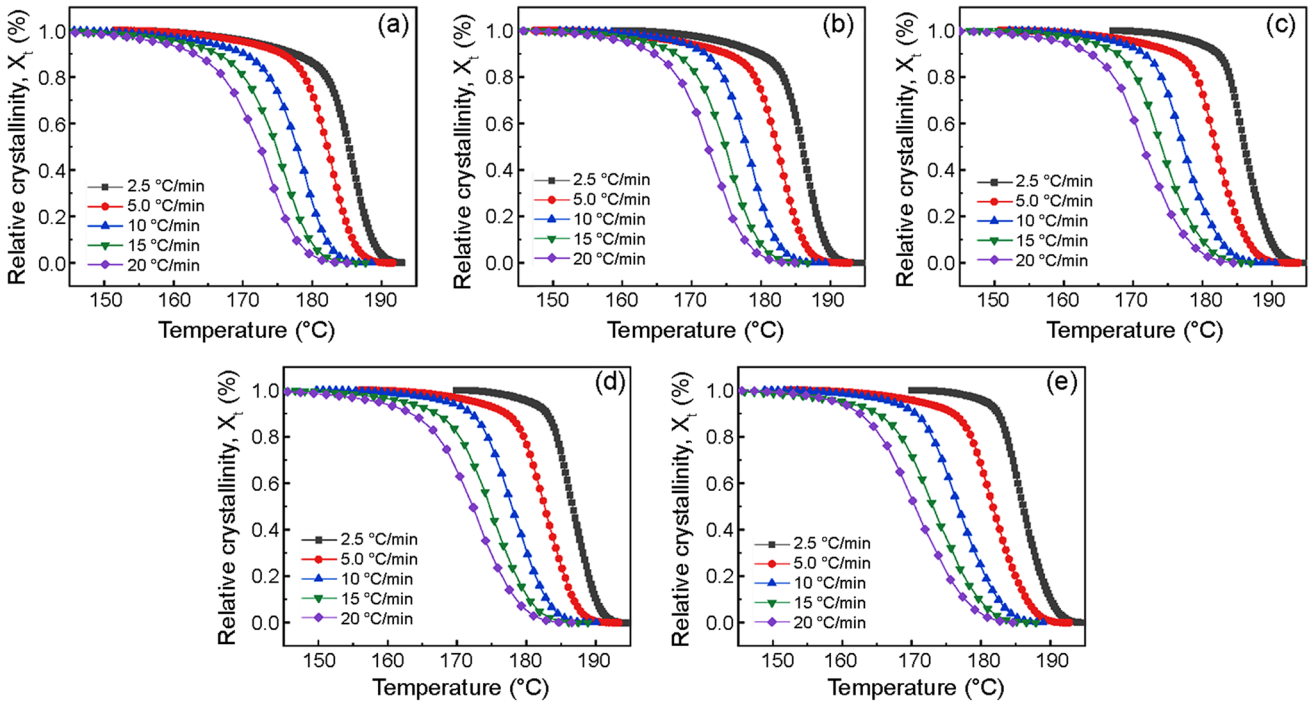

Fig. 5 Relative degree of crystallinity ($X(T)$) versus temperature at different cooling rates: **a** S0, **b** S1, **c** S2, **d** S3, and **e** S4

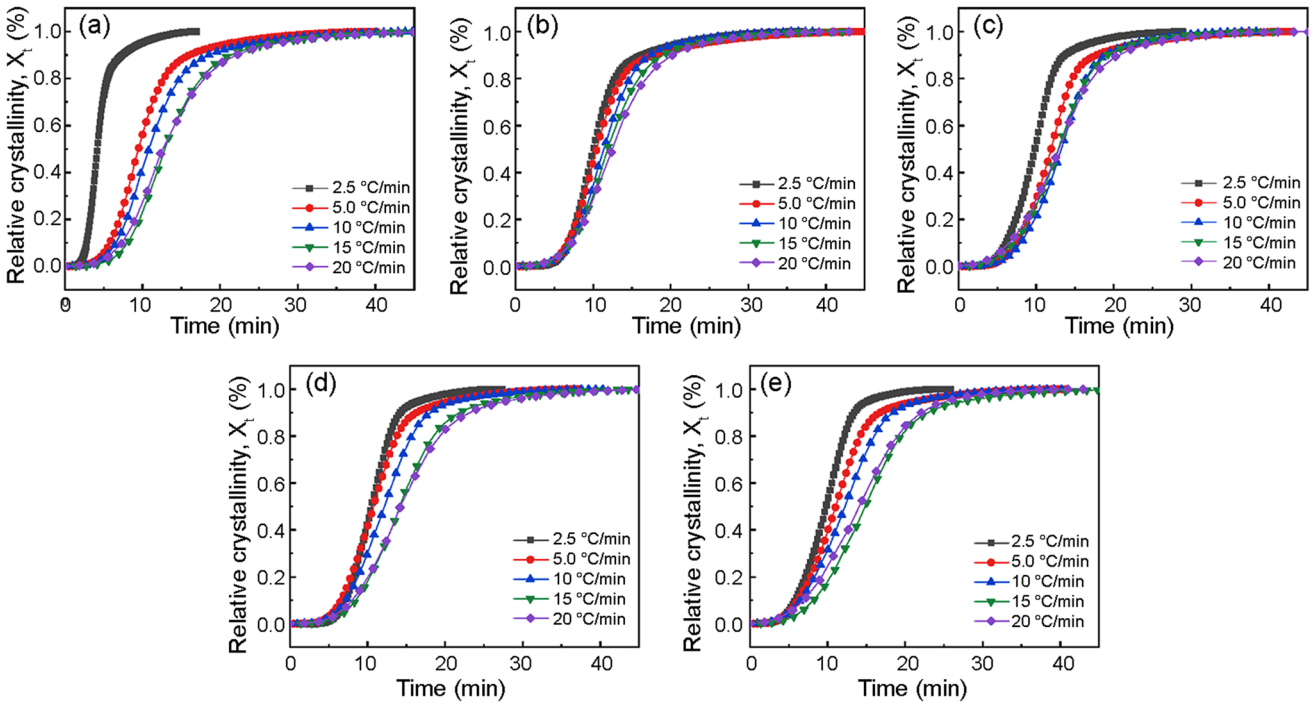

Fig. 6 Relative degree of crystallinity ($X(t)$) versus time at different cooling rates: **a** S0, **b** S1, **c** S2, **d** S3, and **e** S4

by modifying the Avrami equation. In this paper, Jeziorny model [19] and Mo model [20, 21, 34, 35] were used to analyze, independently.

Jeziorny model

Crystallization kinetics is often investigated and analyzed by Avrami model according to the following equations [36, 37]:

$$1 - X(t) = \exp\left(-Zt^{n}\right) \tag{5}$$

$$\log\left[-\ln((1 - X(t))\right] = \log Z + n\log(t). \tag{6}$$

The values of the Avrami exponent (n) and the rate parameter (Z) can be determined from the slope and intercept of the plot of $\log[-\ln(1 - X(t))]$ versus $\log(t)$. The Avrami exponent indicates the mechanism of nucleation and crystal growth dimensions, whereas Z determines the crystallization rate. In a non-isothermal condition, these parameters have different physical concepts, because temperatures are constantly changing. Considering the effect of cooling rate, the crystallization rate constant (Z) can be modified by the following equation [19, 38]:

$$\log Z_{c} = (\log Z)/\phi. \tag{7}$$

In Eq. 7, Z_c is the modified crystallization rate constant, and the semi-crystallization time, $t_{1/2} = (\ln 2/Z_c)^{1/n}$, is further calculated [39]. The larger the value $t_{1/2}$ is, the slower the crystallization rate is.

The modified Avrami equation (Jeziorny model) can be applied to experimental data to obtain the corresponding crystallization kinetic parameters. The results of Jeziorny model for MC nylon 6 and PPES/MC nylon 6 in-situ composites are presented in Fig. 7. As seen, the crystallization behavior exhibits two regimes of primary and secondary crystallizations. In the primary crystallization, it has a good linear relationship between $\log[-\ln(1 - X(t))]$ and $\log(t)$ (its linear fitting results are shown in Fig. 8). While in the secondary crystallization, the free growth of crystals is restricted due to the collision between the crystals, which makes the curve deviate obviously [40]. The obtained model parameters are presented in Table 2.

Based on the data obtained from Jeziorny model, MC nylon 6 has a slow crystallization rate with Z_c values changing from 0.052 to 1.048 and n values of about four, which demonstrate a 3D spherulitic growth mechanism for MC nylon 6 crystallization. By adding PPES to MC nylon 6, the mechanism of nucleation and crystal growth dimensions change slightly as the n values have not changed significantly while distinctively for the composite containing 8% PPES [17, 41, 42]. In addition, with the increase of cooling rate, the Z_c of MC nylon 6 and its in-situ composites gradually increase, and their semi-crystallization times $t_{1/2}$ decrease.

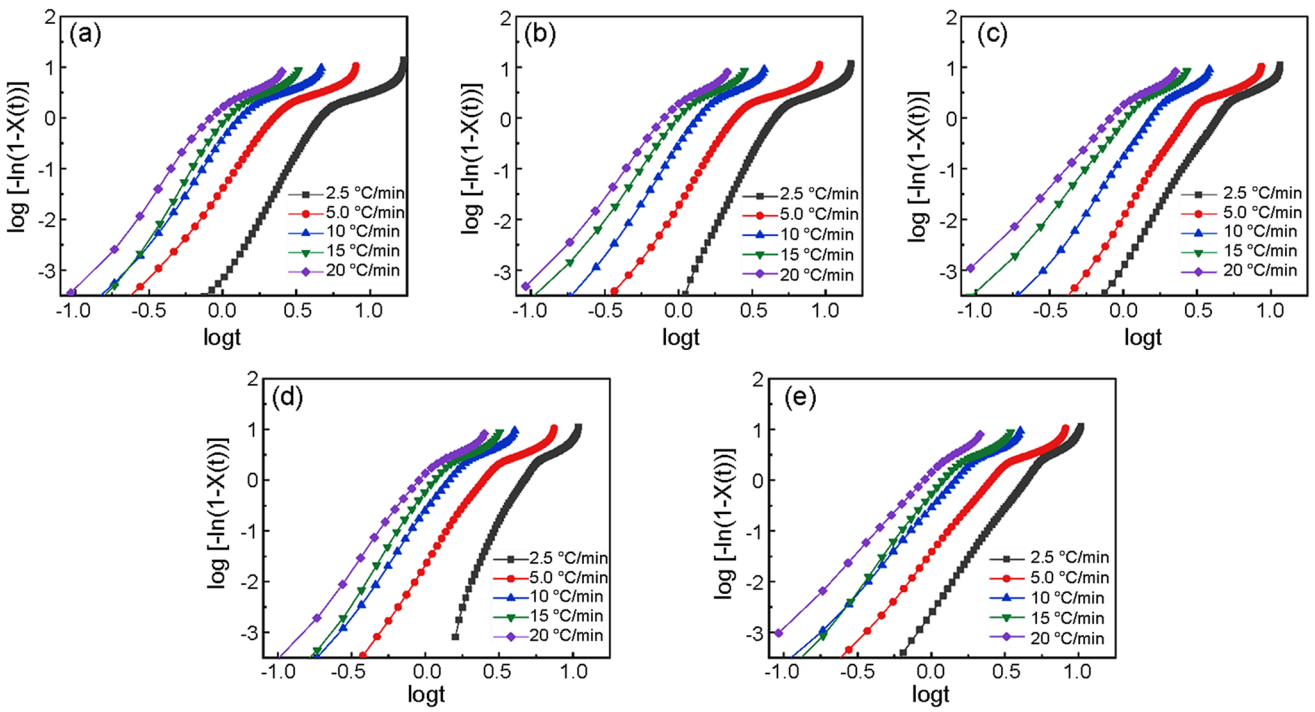

Fig. 7 Plots of $\log[-\ln(1\text{-}X(t))]$ versus $\log(t)$ based on Jeziorny model: **a** S0, **b** S1, **c** S2, **d** S3, and **e** S4

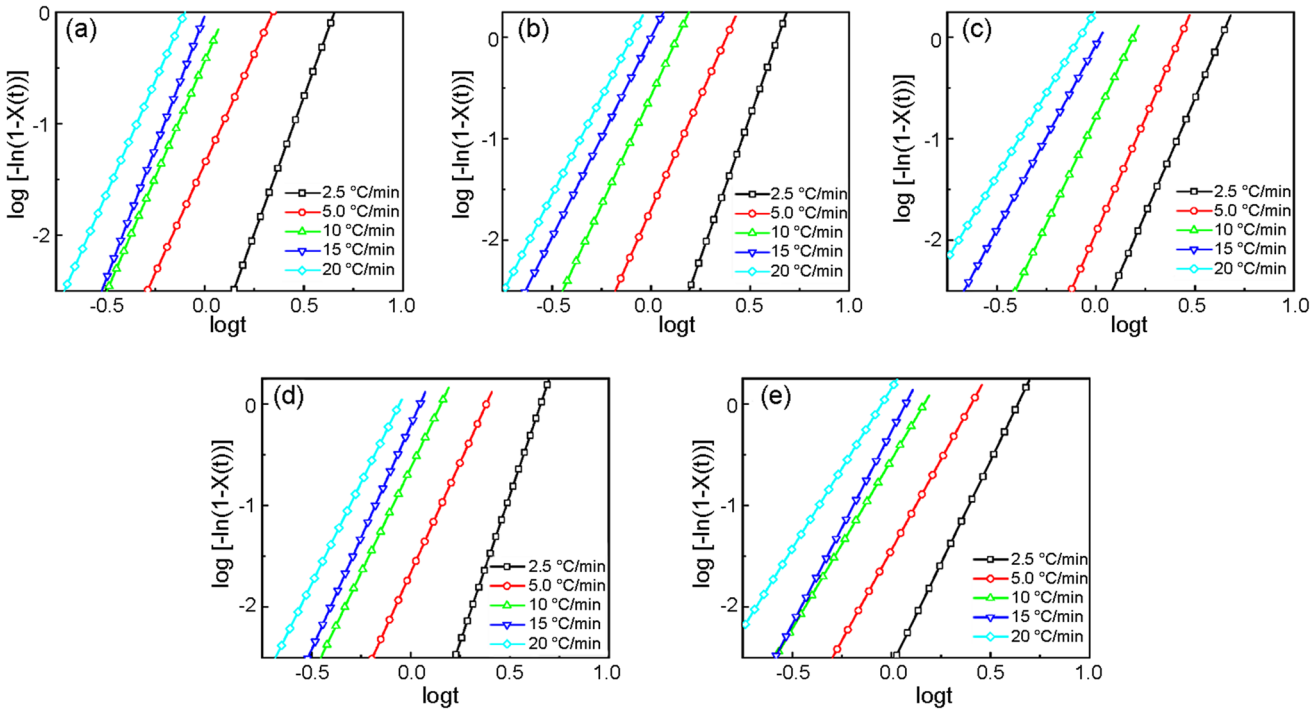

Fig. 8 Curves of linear fitting of primary crystallization using Jeziorny model: **a** S0, **b** S1, **c** S2, **d** S3, and **e** S4

From the data reported in Table 2, the lower values of Z_c for the in-situ composites as compared to those of the neat MC nylon 6 indicate that MC nylon 6 crystallization process becomes slower in the presence of PPES. We explain from the following viewpoints. Cheng et al. [43] believed that the adsorption of macromolecular chains on the heterogeneous surface would reduce the mobility of the chain segments and hinder the transport of macromolecules from the melt to the crystalline region, thus reducing the crystallization rate. From the perspective of thermodynamics, Ebengou [44] believed that when macromolecular chains are adsorbed on the pre-existing heterogeneous surface, the conformational entropy of the chains decreases, which reduces the free energy of the nucleation process and increases the crystallization rate. Combined with Cheng's viewpoint, Ebengou believed that the adsorption of macromolecular chains on the heterogeneous surfaces can reduce the activity of the chain segments and hinder the crystallization. On the other hand, it can reduce the conformational entropy of the chain and promote crystallization, so the final result depends on the synergistic effect of the two factors. In this work, PPES acts as a nucleating agent in the nucleation stage and restricts the movement of chain segments for MC nylon 6 during crystal growth. These findings are in line with the non-isothermal crystallization behavior results.

Mo model

Mo Zhishen et al. combined Ozawa and Avrami equations and proposed a new dynamic model [45, 46]:

$$\log(\phi) = \log F(T) - a\log(t). \tag{8}$$

In Eq. 8, $F(T) = [P(T) - Z]^{1/m}$ is the ratio of the cooling rate to Z, and $a = n/m$ is the ratio of the Avrami to Jeziorny exponents. Based on this relationship at each cooling rate, the changes in the degree of crystallinity are determined. By fitting this relationship on the experimental data, the parameters $F(T)$ and a can be obtained from the intercept and the slope of the lines, respectively. The parameter $F(T)$ has a definite physical and practical meaning and is the value of cooling rate, which has to be chosen at a specific crystallization time to reach a certain degree of crystallinity. A lower $F(T)$ value implies that the system needs a shorter time to develop a certain degree of crystallinity, and it has a higher rate of crystallization. Figure 9 exhibits the lines obtained from fitting the Mo model on the experimental data.

As it is seen from the data presented in Table 3, the a values remain close to unity, indicating that the ratio of the Avrami–Ozawa exponents remains almost unchanged, which confirms that both the models propose the same

Table 2 Non-isothermal kinetic parameters of MC nylon6 and PPES/MC nylon 6 in-situ composites

Samples	ϕ (°C/min)	n	Z (min^{-n})	Z_c (min^{-n})	$t_{1/2}$
S0	2.5	4.90	6.20E−04	0.052	1.70
	5	3.94	0.044	0.535	1.07
	10	4.18	0.364	0.904	0.94
	15	4.75	0.933	0.995	0.93
	20	4.10	2.563	1.048	0.90
S1	2.5	5.56	2.74E−04	0.038	1.69
	5	4.46	0.020	0.458	1.10
	10	4.32	0.266	0.876	0.95
	15	3.94	1.003	1.000	0.91
	20	3.87	2.393	1.045	0.90
S2	2.5	4.54	1.34E−03	0.071	1.65
	5	4.54	0.012	0.411	1.12
	10	4.21	0.163	0.834	0.96
	15	3.64	0.841	0.988	0.91
	20	3.27	1.854	1.031	0.89
S3	2.5	5.77	1.65E−04	0.031	1.72
	5	4.35	0.022	0.465	1.10
	10	4.12	0.235	0.865	0.95
	15	4.43	0.620	0.969	0.93
	20	4.00	1.687	1.026	0.91
S4	2.5	4.05	2.61E-03	0.093	1.64
	5	3.57	0.036	0.515	1.09
	10	3.33	0.282	0.881	0.93
	15	3.80	0.535	0.959	0.92
	20	3.16	1.428	1.018	0.89

mechanism for crystal growth. While the F(T) values of the composites are generally higher as compared to the pure MC nylon 6. This implies that PPES/MC nylon 6 in-situ composites need a longer time to develop a certain degree of crystallinity, and therefore, they have a lower rate of crystallization as compared to the MC nylon 6. This finding corroborates the previous results regarding the role of PPES in acting as a nucleating agent in the nucleation stage and restricting the movement of chain segments for MC nylon 6 during crystal growth.

Activation energy of non-isothermal crystallization

The activation energy for a non-isothermal crystallization process can be calculated based on several methods presented by Augis and Bennett [47], Kissinger [48], Friedman [49], and Takhor [50].

Friedman method

According to the Friedman method:

$$\ln\left(\frac{dX}{dt}\right)_{X,j} = \text{const} - \frac{\Delta E_X}{RT_{x,j}}, \tag{9}$$

where dX/dt is the ratio of changes in the relative degree of crystallinity with time, and ΔE_X is the crystallization activation energy at a certain degree of crystallinity. To obtain ΔE_X, one needs to determine dX/dt. The dX/dt values for all the studied samples were determined. According to Eq. 9, from the plots of ln(dX/dt) versus $1/RT_x$, the activation energies can be obtained from the slopes of the straight lines fitted on the experimental data. Therefore, for each value of the relative degree of crystallinity, the Friedman equation was fitted on the data and the obtained Friedman lines for MC nylon6 and PPES/MC nylon 6 in-situ composites are presented in Fig. 10. Accordingly, the variations of activation energy against the relative degree of crystallinity and average temperature for all the studied samples are shown in Fig. 11. It is found that the values of ΔE_X are negative as expected. From these figures, it can be inferred that the presence of PPES in the MC nylon 6 matrix has reduced the crystallization activation energy, which can be attributed to PPES in the MC nylon 6 matrix that can act as heterogeneous nucleating agent, and can promote the formation of MC nylon 6 crystal nucleus. In addition, with the increase of crystallinity, all the absolute values of ΔE_X of MC nylon6 and PPES/MC nylon 6 in-situ composites decrease. In addition, with the increase of temperature, all the absolute values of ΔE_X of MC nylon 6 and PPES/MC nylon 6 in-situ composites increase. The activation energy sign indicates that crystallization gradually becomes easy with the decreasing crystallization temperature.

Kissinger method

Also, the activation energy of non-isothermal crystallization is usually analyzed by Kissinger method [26, 51–54], and the formula is as follows:

$$\ln\left(\phi/T_c^2\right) = \frac{-\Delta E}{R}\left(1/T_c\right). \tag{10}$$

In Eq. 10, ϕ is the cooling rate, T_c is the corresponding crystallization peak temperature at a specific cooling rate, ΔE is the activation energy of non-isothermal crystallization

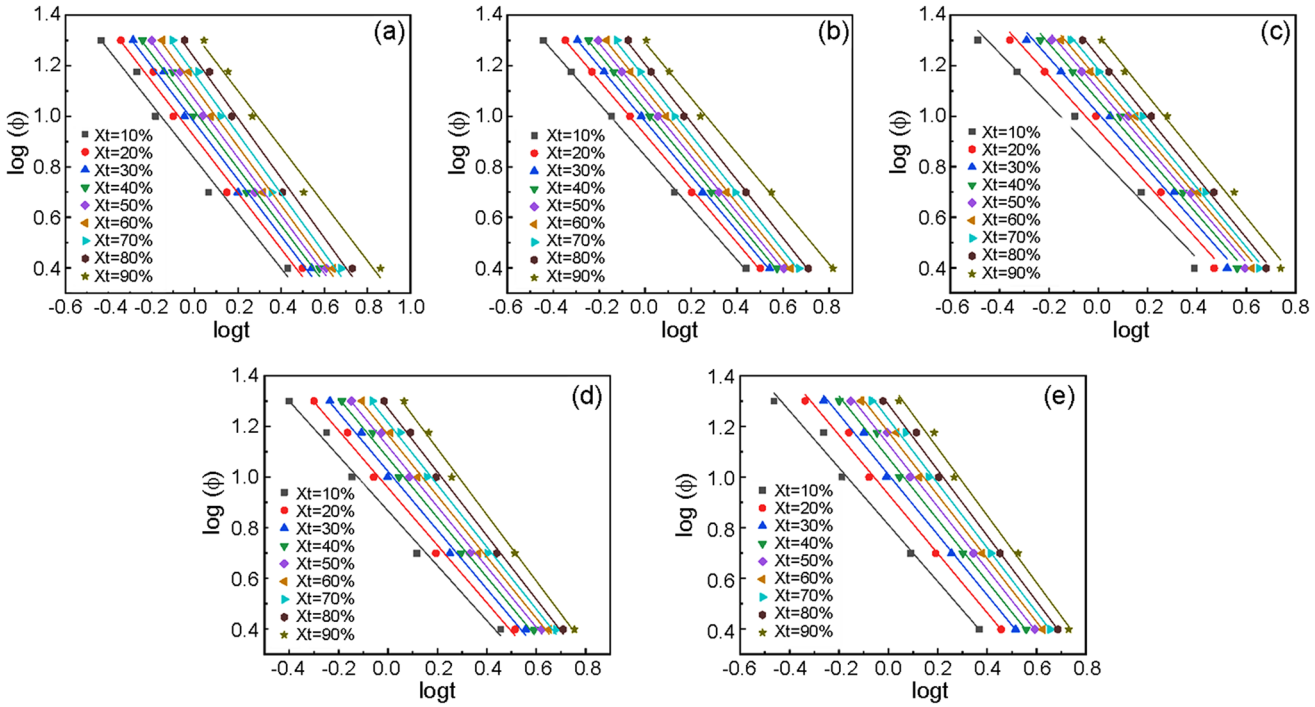

Fig. 9 Plots of log(ϕ) versus log(t) based on Mo model: **a** S0, **b** S1, **c** S2, **d** S3, and **e** S4

Table 3 Crystallization kinetic parameters obtained based on Mo model at different relative degrees of crystallinity

Samples	S0		S1		S2		S3		S4	
$X(T)$	a	$F(T)$	a	$F(T)$	a	$F(T)$	a	$F(T)$	a	$F(T)$
10%	1.08	6.77	1.03	6.98	1.02	6.98	1.08	7.36	1.12	6.49
20%	1.11	8.27	1.07	8.45	1.08	8.80	1.13	9.07	1.17	8.55
30%	1.12	9.42	1.09	9.55	1.10	10.26	1.16	10.54	1.19	10.24
40%	1.13	10.47	1.10	10.59	1.12	11.55	1.18	11.91	1.22	11.91
50%	1.14	11.61	1.12	11.62	1.14	12.78	1.19	13.23	1.24	13.48
60%	1.16	12.98	1.13	12.77	1.16	13.97	1.21	14.71	1.25	15.09
70%	1.18	14.64	1.14	14.16	1.17	15.33	1.23	16.43	1.27	16.95
80%	1.18	16.94	1.15	16.05	1.20	17.23	1.26	18.69	1.30	19.37
90%	1.12	21.14	1.10	19.52	1.21	21.00	1.31	23.63	1.33	23.95

(kJ/mol), and R is the gas constant. The activation energy data of non-isothermal crystallization can be obtained by the slope of the plots of T_c^{-1} versus $\ln(\phi/T_c^2)$. The plots and data obtained are shown in Fig. 12 and Table 4.

Accordingly, it is observed that the crystallization activation energy of MC nylon 6 is 266.94 kJ/mol. As the amount of PPES increases, the absolute values of crystallization activation energy of PPES/MC nylon 6 in-situ composites gradually decrease. Due to the heterogeneous nucleation of PPES and reducing the crystallization barrier energy, it can promote the formation of MC nylon 6 crystal nucleus.

In summary, analysis of crystallization kinetics of the developed systems by various models quantitatively confirmed that inclusion of PPES to MC nylon 6increased the crystallinity, while the crystallization rate was reduced. Analysis of data based on theoretical models revealed that PPES acted as a nucleating agent in the nucleation stage and restricted the movement of chain segments for MC nylon 6

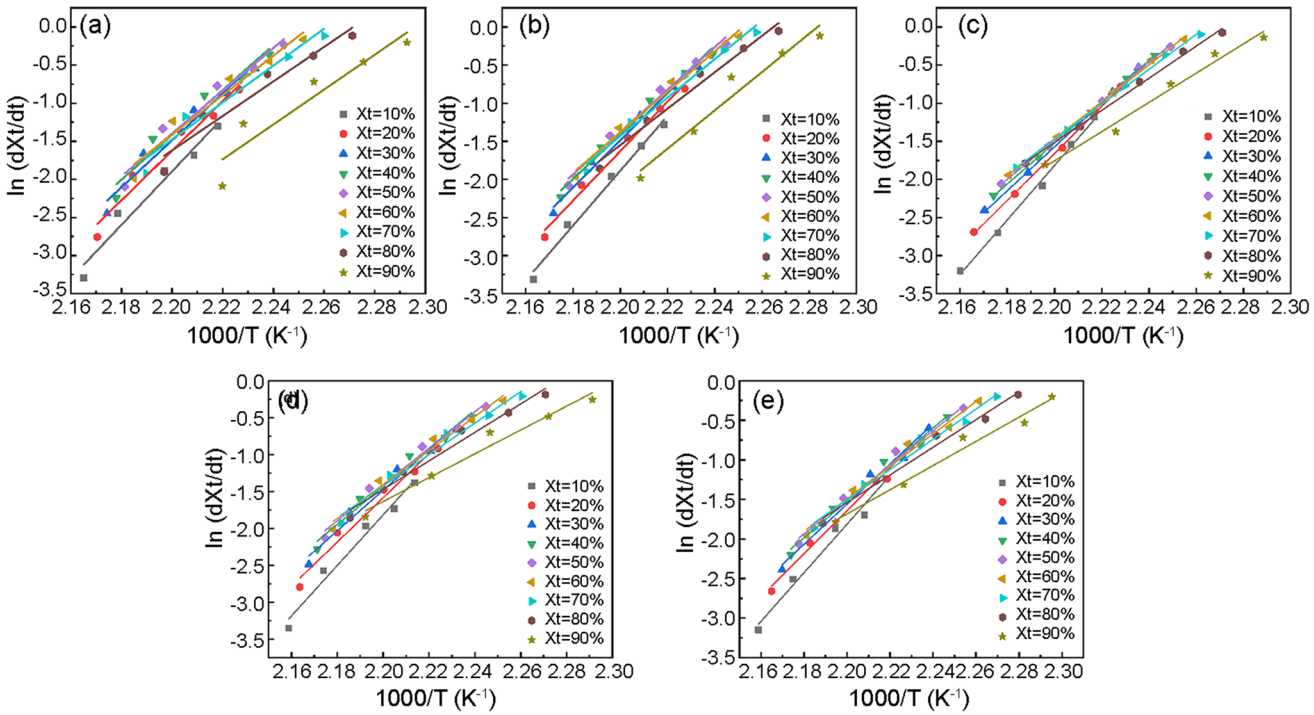

Fig. 10 Friedman plots of ln(d*X*/d*t*) versus $1/RT_x$ at different relative degrees of crystallinity: **a** S0, **b** S1, **c** S2, **d** S3, and **e** S4

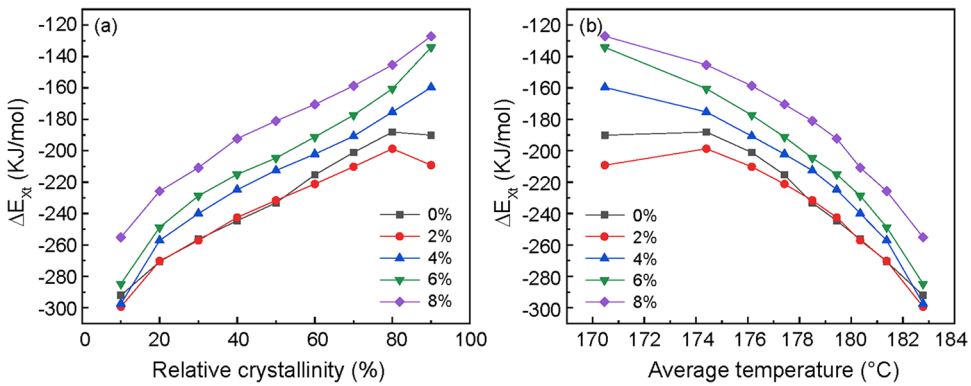

Fig. 11 **a** Dependency of activation energy on degree of crystallization conversion by the Friedman method, and **b** plots of the effective activation energy as function of the average temperature for MC nylon6 and PPES/MC nylon 6 in-situ composites

during crystal growth. Furthermore, the in-situ composites had lower crystallization activation energy compared to MC nylon 6 due to the nucleation effect of PPES.

Conclusions

The hypothesis regarding the sensitivity of crystallization kinetic of MC nylon 6 toward different PPES contents was examined and quantitatively analyzed by various models. Morphological study using SEM revealed PPES particles were well dispersed, at micron levels, in the MC nylon 6 matrix. It was found that inclusion of PPES to MC nylon 6 increased the crystallinity, while the crystallization rate was reduced. Crystallization kinetic studied by Jeziorny model revealed two levels of primary and secondary crystallization mechanisms for all samples. The lower values of Z_c for the in-situ composites as compared to those of MC nylon 6 indicated that MC nylon 6 crystallization process becomes slower in the presence of PPES. The $F(T)$ values of the composites are generally higher as compared to those of pure MC nylon 6, indicating that the interaction between PPES and MC nylon 6 matrix was stronger and the mobility of the polymer molecular chain was difficult. Moreover, the activation energies of crystallization of the in-situ composites were lower than that of MC nylon 6. Analysis of data based on theoretical models revealed that PPES acts as a nucleating agent in the nucleation stage and restricts the movement of chain segments for MC nylon 6 during crystal growth.

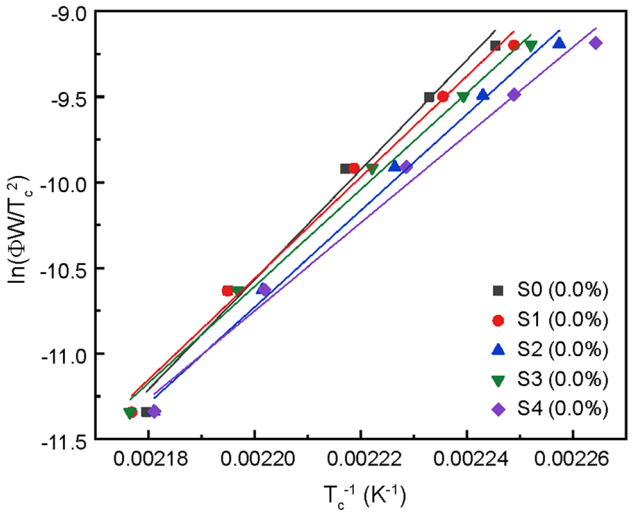

Fig. 12 Plots of T_c^{-1} versus $\ln(\phi/T_c^2)$ by Kissinger equation

Table 4 Activation energy of crystallization obtained based on Kissinger method

Samples	ΔE/(kJmol^{-1})	r^2/%
S0	– 266.94	0.982
S1	– 245.78	0.987
S2	– 234.02	0.991
S3	– 234.74	0.992
S4	– 213.64	0.985

Acknowledgements This work was supported by Funding of Laboratory of Polymer Processing Engineering, Hua Qiao University, Talent Introduction Fund of Fujian Province.

References

1. Zhang DZ, Shi H, Zhang XT, Kan Z (2021) In-situ preparation and performance of MC nylon 6/cellulose nanocrystalline composites (in Chinese). Eng Plast Appl 49:1–7
2. Wang WQ, Ying J, Wang JK, Wang Q (2019) The influence of montmorillonite on the processing and properties of anionic polyamide 6/montmorillonite composites via vacuum assisted resin infusion. Polym Compos 40:1481–1491
3. Ding WJ, Wang YM, Ying J, Li Y, Liu HL, Yuan X, Yu H, Wang JK (2020) Simultaneous enhancements of mechanical and thermal properties of monomer cast nylon via polydimethylsiloxane-modified kaolin. Polym Compos 41:494–504
4. Yang F, Gao YB, Mutua FN, Dong YS, He Y (2018) Preparation and properties of carbon fiber reinforced MC nylon 6 composites by in-situ polymerization (in Chinese). Dev Appl Mater 33:90–95
5. Taki K, Suenaga H, Ito H (2018) Effect of thermal annealing on crystallinity and mechanical strength of textile glass and carbon fiber reinforced in situ polymerized epsilon-caprolactam parts. Microsyst Technol 24:663–668
6. Jian XG, Liao GX, Wang JY (2002) Research progress of poly(arylene ether ketone)s and poly(arylen ether sulfone)s containing phthalazinone moieties (in Chinese). China Plast 16:11–14
7. Liu WB, Wang RG, Zhang HT, Jia J, Jiao WC, Xie HQ (2004) High temperature mechanical properties of CF/PPEK and CF/PPES composites. Mater Sci Technol 12:183–189
8. Zhang MQ (2006) Research on mechanical properties at high and low temperature of high performance thermoplastic composites (in Chinese). Harbin Institute of Technology
9. Zhang PF (2014) In-situ preparation of PPES/MCPA6 and its modification to the PPES, PPES/PA6 systems (in Chinese). Huaqiao University
10. Yao HM, Lin ZY, Li BX, Tong CQ (2008) Effect of interaction between PPES and MC nylon 6 on MC nylon 6 crystallization and melting behavior of PPES/MC nylon6 blends (in Chinese). Chem Eng 12:40–43
11. Papageorgiou DG, Papageorgiou GZ, Bikiaris DN, Chrissafis K (2013) Crystallization and melting of propylene-ethylene random copolymers:homogeneous nucleation and nucleating agents. Eur Polym J 49:1577–1590
12. Mu D, Yuan WZ, Sheng M, Chen YB (2012) Crystallization behavior and mechanical properties of nylon 66/GF composite (in Chinese). Plastics 41:57–59
13. Liu XH, Fan JQ, Qi ZN (2001) Study on non-isothermal crystallization kinetics of polypropylene/montmorillonite nanocomposites (in Chinese). Polym Mater Sci Eng 17:103–105
14. Alvaredo A, Martín M, Castell P, Roberto G, Fernández-Blázquez J (2019) Non-isothermal crystallization behavior of PEEK/graphene nanoplatelets composites from melt and glass states. Polymers 11:124
15. Wunderlich B (1980) Macromolecular physics, vol. 3, crystal melting. Academic, New York
16. Chen Z, Yao C, Yang G (2012) Nonisothermal crystallization behavior, and morphology of poly (trimethylene terephthalate)/polyethylene glycol copolymers. Polym Test 31:393–403
17. Avrami M (1940) Kinetics of phase change: II transformation-time relations for random distribution of nuclei. J Chem Phys 8:212–224
18. Ozawa T (1971) Kinetics of non-isothermal crystallization. Polymer 12:150–158
19. Jeziorny A (1978) Parameters characterizing the kinetics of the non-isothermal crystallization of poly (ethylene terephthalate) determined by DSC. Polymer 19:1142–1144
20. Liu JP, Mo ZS (1991) Crystallization kinetics of polymer (in Chinese). Polym Bull 4:199–207
21. Liu T, Mo Z, Wang S, Zhang H (1997) Nonisothermal melt and cold crystallization kinetics of poly(ary1 ether ether ketone ketone). Polym Eng Sci 37:568–575
22. Weng WG, Chen GH, Wu DJ (2003) Crystallization kinetics and melting behaviors of nylon 6/foliated graphite nanocomposites. Polymer 44:8119–8132
23. Cai LF, Qian H, Lin ZY, Lan XR (2004) Non-isothermal crystallization kinetics of silica/MC nylon 6 in-situ nano-scale composites (in Chinese). China Plast Ind 32:41–43
24. Ribeiro B, Hein L, Costa ML, Pötschke P, Burkhart T, Botelho EC (2017) Nonisothermal crystallization kinetic study and thermal stability of multiwalled carbon nanotube reinforced poly (phenylene sulfide) composites. Polym Compos 38:604–615
25. Jafari S, Khajavi R, Goodarzi V, Kalaee MR, Khonakdar HA (2019) Nonisothermal crystallization kinetic studies on melt processed poly(ethylene terephthalate)/polylactic acid blends containing graphene oxide and exfoliated graphite nanoplatelets. J Appl Polym Sci 136:47569

26. Jebril S, Doudou BB, Zghal S, Dridi C (2019) Non-isothermal crystallization kinetics of hybrid carbon nanotube-silica/polyvinyl alcohol Nanocomposites. J Polym Res 26:1–11
27. Lv C, Liu DG, Tian HF, Xiang AM (2020) Non-isothermal crystallization kinetics of polyvinyl alcohol plasticized with glycerol and pentaerythritol. J Polym Res 27:1–7
28. Yu F, Xiao L (2021) Non-isothermal crystallization kinetics of poly(ether sulfone) functionalized graphene reinforced poly(ether ether ketone) composites. Polym Test 97:107150
29. Chen D, Lei L, Zou M, Li X (2021) Non-isothermal crystallization kinetics of poly (ethylene glycol)-poly (l-lactide) diblock copolymer and poly (ethylene glycol) homopolymer via fast-scan chip-calorimeter. Polymers 13:1156
30. Guo J, Liu M, Wang H, Yu Y (2021) Non-isothermal crystallization kinetics of polypropylene/bamboo fiber/nano-TiO_2 composites. Polym Compos 42:2531–2543
31. Alghamdi AA, Alattas H, Saeed WS, Al-Odayni AB, Ahmed AYBH, Al-Owais AA, Aouak T (2021) Thermal properties, isothermal decomposition by direct analysis in real-time-of-flight mass spectrometry and non-isothermal crystallization kinetics of poly (ethylene-*co*-vinyl alcohol)/poly (*ε*-caprolactone) blend. Curr Comput-Aided Drug Des 11:292
32. Qiao Y, Jalali A, Yang J, Chen Y, Wang S, Jiang Y, Park CB (2021) Non-isothermal crystallization kinetics of polypropylene/polytetrafluoroethylene fibrillated composites. J Mater Sci 56:3562–3575
33. Borhan A, Taib RM (2020) Non-isothermal crystallization kinetics of poly (lactic acid)/kenaf fiber composites. Sains Malays 49:2169–2185
34. Mo ZS (2008) A method for the non-isothermal crystallization kinetics of polymers (in Chinese). Acta Polym Sin 7:656–667
35. Aziz AMS, Naguib HF, Saad GR (2014) Non-isothermal crystallization kinetics of bacterial poly (3-hydroxybutyrate) in poly (3-hydroxybutyrate-*co*-butylene adipate) urethanes. Thermochim Acta 591:130–139
36. Eder M, Wlochowicz A (1983) Kinetics of non-isothermal crystallization of polyethylene and polypropylene. Polymer 24:1593–1595
37. Bhattarai N, Kim HY, Dong IC, Lee DR, Dong IY (2003) Nonisothermal crystallization and melting behavior of the copolymer derived from *p*-dioxanone and poly (ethylene glycol). Eur Polym J 39:1365–1375
38. Chen S, Jin J, Zhang J (2011) Non-isothermal crystallization behaviors of poly (4-methyl-pentene-1). J Therm Anal Calorim 103:229–236
39. Yang JL, Zhao T, Cui JJ, Liu LJ, Zhou YC, Li G, Zhou EL, Chen XS (2010) Nonisothermal crystallization behavior of the poly(ethylene glycol) block in poly (*L*-lactide)-poly (ethylene glycol) diblock copolymers: effect of the poly (*L*-lactide) block length. J Polym Sci Part B 44:3215–3226
40. Wang ZQ, Hu GS, Zhang JT, Xu JS, Shao ZJ (2017) Study on non-isothermal crystallization kinetics of high-temperature resistant polyamides prepared by melt polymerization (in Chinese). Mater Rep 31:161–170
41. Avrami M (1939) Kinetics of phase change: I—general theory. J Chem Phys 7:1103–1112
42. Avrami M (1941) Kinetics of phase change: III—granulation, phase change and microstructure. J Chem Phys 9:177–184
43. Cheng S, Shanks RA (1993) The crystallization kinetics of filled poly (ethylene terephthalate). J Appl Polym Sci 47:2149–2160
44. Ebengou RH (1997) Adsorption as a mechanism for nucleating activity: A thermodynamic explanation. J Polym Sci Part B 35:1333–1338
45. Qiu Z, Yang W (2010) Nonisothermal melt and cold crystallization kinetics of poly (aryl ether ether ketone ketone). Polym Eng Sci 37:568–575
46. Supaphol P, Dangseeyun N, Srimoaon P, Nithitanakul M (2003) Nonisothermal melt-crystallization kinetics for three linear aromatic polyesters. Thermochim Acta 406:207–220
47. Augis JA, Bennett JE (1978) Calculation of the Avrami parameters for heterogeneous solid state reactions using a modification of the Kissinger method. Thermal Anal 13:283–292
48. Kissinger HE (1956) Variation of peak temperature with heating rate in differential thermal analysis. J Res Natl Bur Stand 57:217–221
49. Friedman HL (1964) Kinetics of thermal degradation of char-forming plastics from thermogravimetry:application to a phenolic plastic. J Polym Sci Part C 6:183–195
50. Takhor RL (1971) Advances in nucleation and crystallization of glasses. American Ceramics Society, Columbus, pp 166–172
51. Selvi J, Parthasarathy V, Mahalakshmi S, Anbarasan R, Daramola MO, Kumar PS (2020) Optical, electrical, mechanical, and thermal properties and non-isothermal decomposition behavior of poly(vinyl alcohol)-ZnO nanocomposites. Iran Polym J 29:411–422
52. Mahalakshmi S, Kannammal L, Tung KL, AnbarasanR PV, Alagesan T (2019) Evaluation of kinetic parameters for the crystallization and degradation process of synthesized strontium mercaptosuccinate functionalized poly(*ε*-caprolactone) by non-isothermal approach. Iran Polym J 28:549–562
53. Chen CW, Hsu TS, Huang KW, Rwei SP (2020) Effect of 1, 2, 4, 5-benzenetetracarboxylic acid on unsaturated poly (butyleneadipate-*co*-butylene itaconate) copolyesters: synthesis, non-isothermal crystallization kinetics, thermal and mechanical properties. Polymers 12:1160
54. Vyazovkin S (2015) Is the Kissinger equation applicable to the processes that occur on cooling? Macromol Rapid Commun 23:771–775

Authors and Affiliations

Huimei Yao[1] · Wei Li[1] · Zhen Zeng[1] · Tao Wang[1] · Jingrui Zhu[1] · Zhiyong Lin[2]

✉ Huimei Yao
13860202695@126.com

[1] Ji'an Vocational and Technical College, Ji'an 343000, Jiangxi, China

[2] College of Material Science and Engineering, Hua Qiao University, Xiamen 361021, China